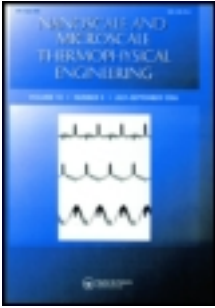


This article was downloaded by: [University of Virginia, Charlottesville]

On: 28 December 2012, At: 14:13

Publisher: Taylor & Francis

Informa Ltd Registered in England and Wales Registered Number: 1072954 Registered office: Mortimer House, 37-41 Mortimer Street, London W1T 3JH, UK



Nanoscale and Microscale Thermophysical Engineering

Publication details, including instructions for authors and subscription information:

<http://www.tandfonline.com/loi/umte20>

Effects of Intra- and Interband Transitions on Electron-Phonon Coupling and Electron Heat Capacity After Short- Pulsed Laser Heating

Patrick E. Hopkins^a, John C. Duda^b, Richard N. Salaway^b, Justin L. Smoyer^b & Pamela M. Norris^b

^a Engineering Sciences Center, Sandia National Laboratories, Albuquerque, New Mexico, USA

^b Department of Mechanical and Aerospace Engineering, University of Virginia, Charlottesville, Virginia, USA

Version of record first published: 12 Dec 2008.

To cite this article: Patrick E. Hopkins, John C. Duda, Richard N. Salaway, Justin L. Smoyer & Pamela M. Norris (2008): Effects of Intra- and Interband Transitions on Electron-Phonon Coupling and Electron Heat Capacity After Short-Pulsed Laser Heating, *Nanoscale and Microscale Thermophysical Engineering*, 12:4, 320-333

To link to this article: <http://dx.doi.org/10.1080/15567260802591985>

PLEASE SCROLL DOWN FOR ARTICLE

Full terms and conditions of use: <http://www.tandfonline.com/page/terms-and-conditions>

This article may be used for research, teaching, and private study purposes. Any substantial or systematic reproduction, redistribution, reselling, loan, sub-licensing, systematic supply, or distribution in any form to anyone is expressly forbidden.

The publisher does not give any warranty express or implied or make any representation that the contents will be complete or accurate or up to date. The accuracy of any instructions, formulae, and drug doses should be independently verified with primary sources. The publisher shall not be liable for any loss, actions, claims, proceedings, demand, or costs or damages whatsoever or howsoever caused arising directly or indirectly in connection with or arising out of the use of this material.

EFFECTS OF INTRA- AND INTERBAND TRANSITIONS ON ELECTRON-PHONON COUPLING AND ELECTRON HEAT CAPACITY AFTER SHORT-PULSED LASER HEATING

Patrick E. Hopkins¹, John C. Duda², Richard N. Salaway²,
Justin L. Smoyer², and Pamela M. Norris²

¹Engineering Sciences Center, Sandia National Laboratories, Albuquerque,
New Mexico

²Department of Mechanical and Aerospace Engineering, University of Virginia,
Charlottesville, Virginia

This work considers the effects of intra- and direct interband transitions on electron heat capacity and the electron-phonon coupling factor in metals. In the event of an interband transition, the population of the electron bands around the Fermi level will change, affecting the electron density of states and subsequently the thermophysical properties. In the event of photon-induced interband transitions, this repopulation can occur even at relatively low temperatures. This introduces a photon energy-dependent population term into density of states calculations when examining the effects of direct interband transitions on electron heat capacity and the electron-phonon coupling factor in temperature regimes where traditionally only intraband transitions are considered. Example calculations are shown for copper and the two-temperature model is solved using the interband-dependent values of electron heat capacity and electron-phonon coupling factor to examine the effect of these transitions on the transient electron temperature after short-pulsed laser heating.

KEY WORDS: intraband transitions, interband transitions, electron heat capacity, electron-phonon coupling factor, Fermi smearing, two-temperature model, short pulsed laser heating

INTRODUCTION

Electron-phonon energy transfer after short-pulsed laser heating is becoming a critical factor in many nanoscale applications. As characteristic length and timescales continue to decrease, the thermal resistances associated with electron-phonon energy

Received 15 September 2008; accepted 26 October 2008.

This paper was presented at the 6th Japan–U.S. Joint Seminar on Nanoscale Transport Phenomena—Science and Engineering, July 13–16, 2008, Boston, Massachusetts.

Patrick Hopkins gratefully appreciates financial support from the Sandia National Laboratories Harry S. Truman fellowship, and Michael Francis of the Engineering Physics Department at U.Va. for insightful discussions regarding electronic properties of materials. The authors gratefully acknowledge financial support from the Office of Naval Research MURI program, grant #N00014-07-1-0723. The authors thank Matthew Bauer and Michael Fish for critical reading of the manuscript. Sandia is a multiprogram laboratory operated by Sandia Corporation, a Lockheed-Martin Company, for the United States Department of Energy's National Nuclear Security Administration under Contract DE-AC04-94AL85000.

Address correspondence to Patrick E. Hopkins, Engineering Sciences Center, Sandia National Laboratories, P.O. Box 5800, Albuquerque, NM 87185-0346. E-mail: pehopki@sandia.gov

NOMENCLATURE			
A	Absorbed laser fluence, J m^{-2}	t_p	pulse width, s
C	Heat capacity, $\text{J m}^{-3} \text{K}^{-1}$	Greek Symbols	
D	Density of states per unit energy per unit volume, $\text{eV}^{-1} \text{m}^{-3}$	γ	Sommerfeld coefficient, $\text{J m}^{-3} \text{K}^{-2}$
d	Film thickness, m	ε	Energy, eV
G	Electron-phonon coupling factor, $\text{W m}^{-3} \text{K}^{-1}$	ε_F	Fermi energy, eV
G_0	Electron-phonon coupling constant, $\text{W m}^{-3} \text{K}^{-1}$	θ_D	Debye temperature, K
g	Gibbs free energy, eV m^{-3}	λ	Electron phonon mass enhancement parameter
k	Wavevector, m^{-1}	μ	Chemical potential, eV
k_B	Boltzmann's constant, eV K^{-1}	ν	Photon frequency, Hz
h	Planck's constant, eV s	ρ	Mass density, kg m^{-3}
\hbar	Planck's constant divided by 2π , eV s	$\langle \omega^2 \rangle$	Second moment of the phonon spectrum, s^{-2}
ITT	Interband transition threshold	Subscripts	
N	Atomic number density, m^{-3}	d	d-Band
n	Electron number density, m^{-3}	e	Electron
T	Temperature, K	L	Lattice
t	time, s	s	s/p-Band

processes are becoming comparable to typical thermal resistances associated with thermal transport in [1] or across the solid interfaces [2, 3] of devices. With the increasing importance of short-pulsed heating and subsequent electron-phonon processes in fundamental research and engineering applications [4–9], the need to accurately predict the thermophysics associated with these processes is rapidly increasing.

Immediately after partial absorption of an incident laser pulse by the electrons in a solid, the energy of the absorbed photon, $h\nu$, where h is Planck's constant and ν is the photon frequency, causes the electron to excite to a higher energy state. If the excited state is within the same energy band, this excitation is called an intraband transition. If the energy of the absorbed photon is greater than the energy of an allowable excitation between bands, then the excited electron will undergo an interband transition. Since Fermi smearing affects the available energy states within approximately $3k_B T_e$ of the Fermi energy, ε_F , where k_B is Boltzmann's constant and T_e is the electron system temperature [10], the various intra- and interband transitions will relocate electrons to states as low as $1.5 k_B T$ below the Fermi energy to energies as high as the vacuum level, depending on $h\nu$.

The minimum photon energy required to excite an electron to undergo an interband transition to an empty state near the Fermi energy is called the *interband transition threshold* (ITT) [5]. The ITT is dependent on the band structures and relative energies of the outermost filled and innermost partially filled or empty electron bands (relative to the nucleus). Therefore, the ITT is unique for any given material. For semiconductors and insulators, the ITT is the bandgap, and it represents the energy difference between the valence (outermost filled) and conduction (innermost empty) bands. Metals, however, are more complex since electron energy bands can overlap

around the Fermi energy, allowing these bands to be partially filled. This, in fact, is what makes metals better electrical conductors than semiconductors and, consequently, why electron-phonon scattering is such a dominant form of electrical and thermal resistance in metals. In a transition metal, for example, the s-band/d-band crossing is at an energy equal to or greater than the Fermi energy. This produces several allowable low-energy d-band (valence d-band) to s-band interband transitions along with intraband transitions in both the d₁-band and s-band. For example, Cr has interband Fermi transitions at 0.8 (*ITT*), 1.0, 1.4, and 1.6 eV [11]; W has transitions at 0.85 (*ITT*), 1.6, and 1.75 eV [11]; and Ni has transitions at 0.25 (*ITT*), 0.4, and 1.3 eV [12]. This poses experimental difficulty in isolating the effects of interband transitions on electron-phonon coupling [13]. However, noble metals have a very distinct, high-energy *ITT* since the s-band/d-band crossing is significantly lower than the Fermi level, and therefore only the s-band is partially filled. Therefore, the lowest energy d-band to available s-band transition is very large for Cu (2.15 eV), Au (2.4 eV), and Ag (4 eV) [14], making these metals ideal candidates to examine the effects of interband transitions on the thermophysics governing electron-phonon scattering. Figure 1 shows various transitions in a generic noble metal. The energy of the bands is shown as a function of wavevector, k . This schematic represents a noble metal, as there is a large separation of the d-band from the Fermi energy. An intraband transition is depicted as an electron being excited from a state near the Fermi energy in the s/p-band (empty circle) to a higher energy in the same band (filled circle in Figure 1. Note, in intraband transitions, conservation of momentum in k space is upheld through scattering with a phonon [elastically—this process occurs during electron relaxation into the Fermi distribution and the effects on the thermophysical process of electron-phonon coupling analyzed in this article is negligible during the time scale of interest]). The

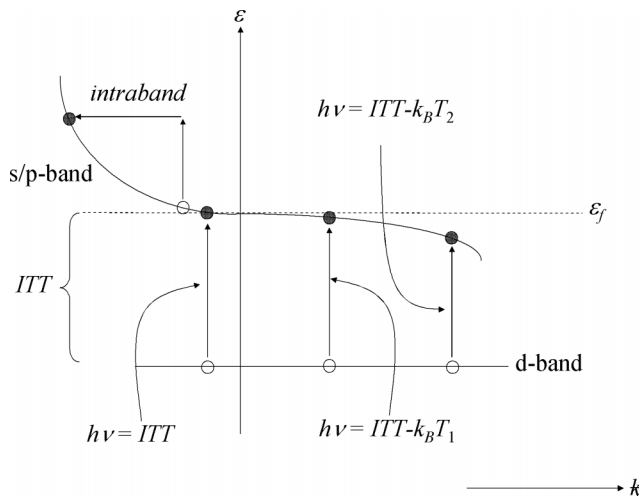


Figure 1. Schematic depicting intraband transition and various interband transitions in a noble metal. Whereas an intraband transition creates an electron/hole pair in the same band, an interband transition creates an electron/hole pair in different bands. The *ITT* is the minimum separation of the d-band from the Fermi energy at $T = 0$. As temperature is increased, photons with energies less than the *ITT* can excite an interband transition due to Fermi smearing which creates empty states in the s/p-band below the Fermi energy.

interband transitions are depicted by the processes in which an electron is excited from the d-band to the s/p-band. These transitions are shown for various temperatures— $T = 0, T_1,$ and T_2 where $T_1 < T_2$ —to illustrate the effects of Fermi smearing on the *ITT*. This will be discussed more quantitatively in the next section.

In this article, the effects of interband transitions, and subsequent repopulation of the s- and d-bands near the Fermi energy, on the temperature dependencies of the electron heat capacity [15], C_e , and electron-phonon coupling factor [16], G , are examined. The following section presents the theory and equations governing C_e and G calculations including thermal and photonic d-band to s-band excitations near the Fermi surface. The section on incidence of thermal and photonic excitations presents calculations of the temperature dependencies of C_e and G for Cu from 300 to 10,000 K. Copper was chosen since its band structure can be approximated with simple functions [17, 18], and the thermal excitations of d-band electrons due to Fermi smearing have been studied with approximate [19] and exact [20] band structure calculations (in addition to the reasons discussed above). The section on transient change in electron temperature uses the temperature-dependent calculations from the preceding section to examine the temporal electron temperature decay after pulse absorption as a function of absorbed photon energy using a two-temperature model (*TTM*) [21].

THEORY

It is well known from free electron theory that the outermost filled s/p-band in metals can be estimated by a parabolic dispersion in $\varepsilon(\mathbf{k})$ space, where $\varepsilon(\mathbf{k})$ is the energy as a function of wavevector, \mathbf{k} [22]. From this, the density of states per unit energy per unit volume in the parabolic valence band can be estimated by [22]:

$$D_s(\varepsilon) = \frac{3n_s}{2} \left(\frac{\varepsilon}{\varepsilon_F} \right)^{1/2} \frac{1}{\varepsilon_F} \quad (1)$$

where n_s is the number of electrons per unit volume in the s/p-band. With Eq. (1), the electronic heat capacity as a function of temperature is calculated by [15]:

$$C_{e,s}(T_e) = \int_0^{\infty} (\varepsilon - \mu(T_e)) D_s(\varepsilon) \frac{\partial f}{\partial T_e} d\varepsilon \quad (2)$$

where f is the Fermi-Dirac distribution function given by:

$$f = \frac{1}{1 + \exp\left[\frac{\varepsilon - \mu(T_e)}{k_B T_e}\right]} \quad (3)$$

where $\mu(T_e)$ is the chemical potential. In the low-temperature limit where the chemical potential is approximately constant at the Fermi energy and the temperature derivative of Eq. (3) is only non-zero near the Fermi energy [17], Eq. (2) simplifies to the familiar expression for specific heat that is linear with temperature and given by:

$$C_{e,s}(T_e) = \gamma T_e \quad (4)$$

where the linear coefficient γ is the Sommerfeld coefficient [23] and calculations of γ agree well with experiments in the noble metals [15] assuming a density of states as given by Eq. (1). Continuing with these density of states and temperature assumptions, the electron-phonon coupling constant can be estimated by [24, 25]:

$$G_0 = \frac{3\hbar\lambda\langle\omega^2\rangle\gamma}{\pi k_B} \quad (5)$$

where λ is the dimensionless electron phonon mass enhancement parameter [26], $\langle\omega^2\rangle$ is the second moment of the phonon spectrum [27], and $\hbar = h/2\pi$. Often, the units of $\langle\omega^2\rangle$ are reported in terms of meV^2 , in which case there is an implied factor of \hbar^2 since the units of $\langle\omega^2\rangle$ in Eq. (5) are s^{-2} . Therefore, given $\langle\omega^2\rangle$ in units of meV^2 , Eq. (5) is recast as

$$G_0 = \frac{3\lambda\langle\omega^2\rangle\gamma}{\pi\hbar k_B}. \quad (6)$$

Considering relatively small electronic excitations that induce only s/p-band intraband transitions around the Fermi level, Eqs. (4) and (5) or (6) hold for evaluating the electron heat capacity and electron-phonon coupling constant using Eq. (1) for the density of states of the s/p-band. The key to evaluating Eqs. (5) and (6) is determining $\mu(T_e)$ in Eq. (3), which is accomplished by evaluating

$$n_s = \int_0^\infty D_s(\varepsilon) f d\varepsilon \quad (7)$$

and iterating $\mu(T_e)$ at various T_e until n_s becomes the constant value for the free electron number density for the metal of interest [22].

In the case of large thermal excitations where Fermi smearing excites electrons in the d-bands to higher energies in the s/p band, Eqs. (5) and (6) must be reevaluated to take into account the d-band's density of states [7, 8, 19, 20]. In this case, Eq. (1) must be recast as

$$D(\varepsilon) = \frac{3n_s}{2} \left(\frac{\varepsilon}{\varepsilon_F} \right)^{1/2} \frac{1}{\varepsilon_F} + D_d(\varepsilon) \quad (8)$$

where $D_d(\varepsilon)$ is the density of states per unit energy per unit volume of the d-bands. The electronic heat capacity as a function of temperature is then calculated by:

$$C_e(T_e) = \int_0^\infty (\varepsilon - \mu(T_e))(D_s(\varepsilon) + D_d(\varepsilon)) \frac{\partial f}{\partial T_e} d\varepsilon. \quad (9)$$

The electron-phonon coupling factor as a function of temperature is evaluated by [28]:

$$G(T_e) = \frac{\pi \hbar k_B \lambda \langle \omega^2 \rangle}{D_s(\varepsilon_F) + D_d(\varepsilon_F)} \int_0^\infty (D_s(\varepsilon) + D_d(\varepsilon))^2 \left(-\frac{\partial f}{\partial \varepsilon} \right) d\varepsilon \quad (10)$$

or, if $\langle \omega^2 \rangle$ is given in units of meV^2 ,

$$G(T_e) = \frac{\pi k_B \lambda \langle \omega^2 \rangle}{\hbar (D_s(\varepsilon_F) + D_d(\varepsilon_F))} \int_0^\infty (D_s(\varepsilon) + D_d(\varepsilon))^2 \left(-\frac{\partial f}{\partial \varepsilon} \right) d\varepsilon. \quad (11)$$

Note that in the case of the noble metals, $D_d(\varepsilon_F) \approx 0$ and at low temperatures (i.e., no thermal d-band excitations) $-\partial f / \partial \varepsilon$ reduces to a delta function centered on the Fermi energy. Therefore, since by free electron theory $\frac{\gamma}{k_B^2 \pi^2} = \frac{n_s}{2\varepsilon_F}$, at low temperatures Eqs. (10) and (11) reduce to Eqs. (5) and (6), respectively [20]. As before, the key to calculations of $C_e(T_e)$ and $G(T_e)$ is determination of $\mu(T_e)$, which, when considering d-band excitations, is accomplished by evaluating

$$n_s + n_d = \int_0^\infty (D_s(\varepsilon) + D_d(\varepsilon)) f d\varepsilon \quad (12)$$

in a similar manner as Eq. (7).

The analysis of Eqs. (8)–(12) takes into account thermal excitations from d-bands to energy states around the Fermi level (those influenced by Fermi smearing). If the electron system is excited with an absorbed energy greater than the ITT ($h\nu \geq ITT$), electrons in the d-bands will be excited to empty states in the s/p-band near the Fermi level through direct interband transitions (for example, excitations that may occur during ultrashort pulse laser irradiation). This will cause a depopulation of the d-band and an increase in the electron number density in the s/p-band near the Fermi energy. This will affect calculations of $\mu(T_e)$, $C_e(T_e)$, and $G(T_e)$ since now there are two competing processes that influence the populations in the s/p-band and the d-bands: (1) thermal excitations resulting in Fermi smearing and promoting electrons in the d-bands up to excited states in the s/p band; and (2) photonic excitations resulting in direct interband transitions also causing a change in the electronic population of the two bands. As the temperature of the electron system increases, empty states will become available below the Fermi level due to Fermi smearing. So at finite temperatures, photonically induced direct interband transitions will occur when $h\nu \geq ITT - 1.5k_B T_e$. Assuming that enough photons are absorbed by the electrons to fill all of the Fermi smearing-induced empty states below the Fermi level, then when the incident photon energy is greater than $ITT - 1.5k_B T_e$, the number of filled states in the valence s/p-band that are populated by electrons from the d-bands below the Fermi level can be approximated by:

$$\begin{aligned}
n_{excited}(h\nu) &= \int_0^{\infty} D_s(\varepsilon)(1-f)(1-H[\varepsilon - \mu(T_e) - (ITT - h\nu)]) \\
&f d\varepsilon, h\nu \geq ITT - 1.5k_B T_e \\
n_{excited} &= 0, h\nu < ITT - 1.5k_B T_e
\end{aligned} \tag{13}$$

where H is the Heaviside function. Therefore, in the event of these interband transitions, the population of the s/p-bands will increase by $n_{excited}$ and the population of the d-bands will decrease by $n_{excited}$. This will affect the density of states in the bands and will alter subsequent calculations of $\mu(T_e)$, $C_e(T_e)$, and $G(T_e)$. As seen in Eq. (13), in this analysis it is assumed that when $h\nu < ITT - 1.5k_B T_e$, no interband excitations will occur [10]; that is, when $h\nu < ITT - 1.5k_B T_e$, $n_{excited} = 0$.

INFLUENCE OF THERMAL AND PHOTONIC EXCITATIONS ON $\mu(T_e)$, $C_e(T_e)$, AND $G(T_e)$ IN Cu

In this section, the theory developed above is used to calculate $\mu(T_e)$, $C_e(T_e)$, and $G(T_e)$. Approximate [19] and exact band [20] structure calculations for Cu give previous results for comparison against the photonic excitation theory developed in this work. Copper has a Fermi energy of $\varepsilon_F = 7.00$ eV [15] and an ITT of 2.15 eV [14]. The electron configuration in the two outermost bands is $3d^{10}4s^1$. The mass density, ρ , of FCC Cu is 8960 kg m^{-3} [22] from which the atomic density, N , is calculated as 8.5×10^{28} m^{-3} . Therefore, the electron densities in the 4s and 3d-bands are $n_s = 8.5 \times 10^{28}$ m^{-3} and $n_d = 8.5 \times 10^{29}$ m^{-3} , respectively. The density of states of the 4s-band is given by:

$$D_s(\varepsilon, h\nu) = \frac{3(8.5 \times 10^{28} + n_{excited})}{14} \left(\frac{\varepsilon}{7}\right)^{1/2} \tag{14}$$

where $n_{excited}$ is given by Eq. (13). The density of states of the 3d band can be approximated by a Gaussian distribution in energy space [18] centered at 3.1 eV below the Fermi energy with a full-width-half-max (FWHM) of 3 eV [18, 19]. The magnitude of the 3d density of states per unit volume is simply n_d and, therefore, the density of states of the 3d band of copper is approximated by:

$$D_d(\varepsilon, h\nu) = \frac{0.94}{3} (8.5 \times 10^{19} - n_{excited}) \exp\left[-2.77\left(\frac{\varepsilon - 3.9}{3}\right)^2\right]. \tag{15}$$

Figure 2 shows the density of states approximations for the $3d^{10}$ and $4s^1$ bands as a function of energy used in these calculations. Also shown in this figure are the temperature trends of the Fermi-Dirac distribution as a function of energy for various temperatures, assuming $\mu(T_e) = \varepsilon_F$ (note that this is not assumed in the actual calculations of $C_e(T_e)$ and $G(T_e)$).

With Eqs. (14) and (15), the chemical potential of Cu is calculated using Eq. (12) and the method described in the previous section. The changes in chemical potential in Cu as a function of temperature are shown in Figure 3 for the cases of: (1) only thermal excitations in the 3d and 4s bands (solid line: d-band thermal

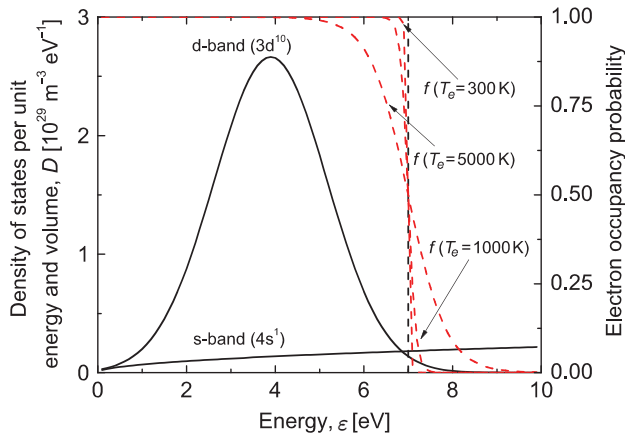


Figure 2. Approximations for the density of states of the $3d^{10}$ and $4s^1$ bands in Cu used in this work. The vertical dashed line represents the Fermi energy (7.00 eV). The dashed lines represent calculations of the Fermi-Dirac distribution function (Eq. (3)) to show the electron occupancy probability as a function of energy at different temperatures. Note that the Fermi-Dirac distribution calculations are simply added as a visual aid to show trends in how empty states below the Fermi energy become available with temperature and assume $\mu(T_e) = \varepsilon_F$. Note that the exact calculations of Eq. (3) used in this work will differ from that shown in this figure due to the different temperature dependencies of $\mu(T_e)$ based on the specific excitation event.

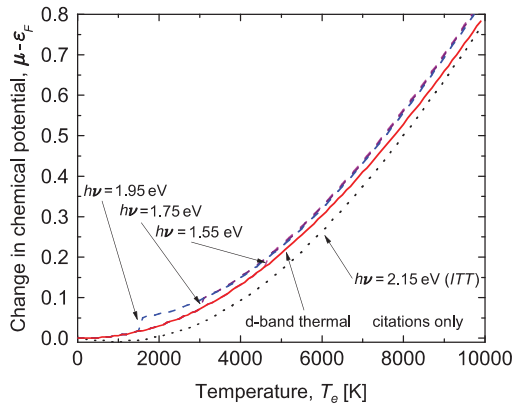


Figure 3. Changes in chemical potential in Cu as a function of temperature for the cases of only thermal excitations in the 3d and 4s bands (solid line: d-band thermal excitations only); sub-ITT photonic excitations causing interband transitions from the 3d band to available states in the 4s band in addition to thermal excitations in the 3d and 4s bands (dashed lines: $h\nu = 1.55$ eV, $h\nu = 1.75$ eV, and $h\nu = 1.95$ eV); and ITT photonic excitations with thermal excitations (dotted line: $h\nu = 2.15$ eV).

excitations only); (2) sub-ITT photonic excitations causing interband transitions from the 3d band to available states in the 4s band in addition to thermal excitations in the 3d and 4s bands (dashed lines: $h\nu = 1.55$ eV, $h\nu = 1.75$ eV, and $h\nu = 1.95$ eV); and (3) ITT photonic excitations with thermal excitations (dotted line: $h\nu = 2.15$ eV). When there is no photonic excitation, $\mu(T_e)$ increases with temperature due to the

number of empty states increasing in the 3d band, in agreement with Lin et al. [20], as opposed to the decrease in $\mu(T_e)$ when considering only the 4s band as predicted from the Sommerfeld expansion [22]. With photonic excitations below the *ITT*, $\mu(T_e)$ sharply increases at $T_e = \frac{ITT - h\nu}{1.5k_B}$ from $\mu(T_e)$ predicted by the d-band thermal excitations only calculations. Note that for the three sub-*ITT* excitations, at T_e , $\mu(T_e)$ is exactly the same as predicted by the d-band thermal excitations only calculations (i.e., the graphs are overlapping in Figure 3). When the photonic excitation is the *ITT*, $\mu(T_e)$ first slightly decreases then continues in a trend exactly parallel to that of the sub-*ITT* excitations.

In the case of d-band thermal excitations only, the increased electron temperature promotes electrons from the high density of states d-band to the low density of states s-band. This causes the increase in chemical potential as opposed to the decrease predicted when only considering the s-band. Thermodynamically, this is intuitive, since the chemical potential is related to the Gibbs free energy, g , through

$$\mu = \frac{g}{n_s + n_d}. \quad (16)$$

Since our overall electron number density in the 3d and 4s bands is not changing during these processes, an increase in chemical potential relates to an increase in Gibbs free energy, which conceptually is a measure of how easily a system can “do work” or “move.” When exciting electrons from the d-band to the s-band, the effective masses of the excited electrons are significantly decreased (flat d-band corresponding to large density of states excited to parabolic/curved s-band corresponding to small density of states) and therefore their mobility, or ability to move, is increased. This increase in μ occurs gradually in the d-band thermal excitations only case since the d-band to s-band promotion is only governed by Eq. (3). However, it appears more abruptly for the sub-*ITT* photonic excitation cases due to the implied condition of no photonic induced interband transitions when $h\nu < ITT - 1.5k_B T_e$. In a more computationally rigorous simulation with more realistic density of states calculations, this discontinuity would be smoother; however, the physical effects of these transitions are still apparent. In the case of $h\nu = 2.15$ eV, d-band electrons are always photonicly excited up to the s-band at all temperatures, and therefore at low temperatures, the change in the population of the s-band mirrors that of free electron theory since the photonic excitations outweigh the thermal excitations. As temperature increases, the relative contribution of thermal excitations increases, creating the increase and inflection point for reasons discussed above.

With the determination of the chemical potential for these various cases, $C_e(T_e)$ and $G(T_e)$ are calculated with Eqs. (9) and (11), respectively. Figure 4 shows calculations of electron heat capacity as a function of temperature for the five excitations shown in the chemical potential calculations in Figure 3. Also included in this graph is the prediction for electron heat capacity based on free electron theory given in Eq. (4) and assuming $\gamma = 96.8 \text{ J m}^{-3} \text{ K}^{-2}$ [15]. The case of d-band thermal excitations only agrees very well with the calculations by Lin et al. [20]. Figure 4 shows that photonicly induced interband transitions will increase the electron heat capacity. The values of $C_e(T_e)$ for the sub-*ITT* interband transitions are exactly the same as the d-band thermal excitations only case until the threshold of the interband transition, at which point the sub-*ITT* calculations follow the trends with very similar values to the *ITT* calculations.

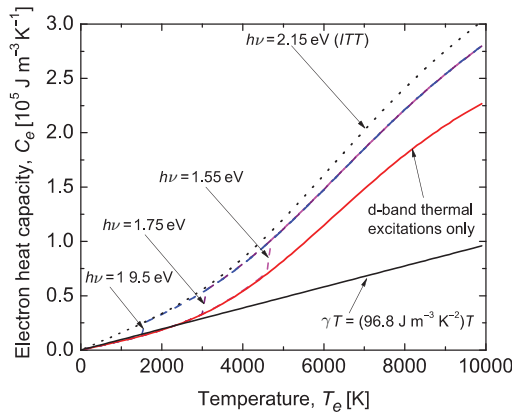


Figure 4. Electron heat capacity as a function of temperature in Cu for the cases of only thermal excitations in the 3d and 4s bands (solid line); sub-ITT photonic excitations causing interband transitions from the 3d band to available states in the 4s band with thermal excitations (dashed lines); ITT photonic excitations with thermal excitations (dotted line); and free electron theory using Eq. (4) (solid line: $\gamma T_e = 96.8 T_e$).

Figure 5 shows calculations of the electron-phonon coupling factor as a function of temperature using Eq. (11) for the five excitation conditions discussed in Figure 3. For these calculations, the experimentally determined value of $\lambda \langle \omega^2 \rangle = 29 \text{meV}^2$ is used [25]. Using Eq. (6), this yields $G_0 = 4.7 \times 10^{16} \text{W m}^{-3} \text{K}^{-1}$. Again, the sub-ITT photonic excited $G(T_e)$ calculations follow those of the d-band thermal excitations only calculations until $T_e = \frac{ITT-h\nu}{1.5k_B}$ (when an interband transition becomes “available”), at which point the $G(T_e)$ calculations follow that of the ITT photonic excited $G(T_e)$. Note that the values of the low-temperature constant $G(T_e)$ predicted by the non-ITT excited calculations are slightly higher than G_0 , which can be ascribed to the density of states assumptions of the s- and d-bands and the numerical solution to

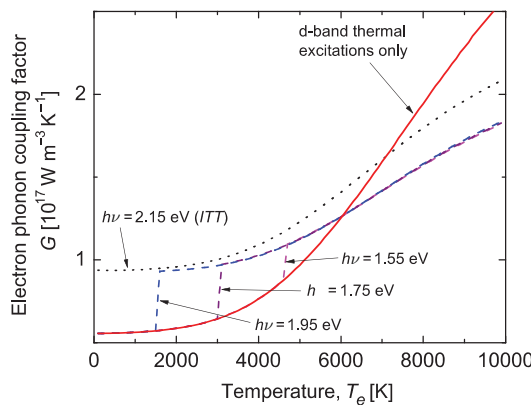


Figure 5. Electron-phonon coupling factor as a function of temperature in Cu for the cases of only thermal excitations in the 3d and 4s bands (solid line); sub-ITT photonic excitations causing interband transitions from the 3d band to available states in the 4s band with thermal excitations (dashed lines); ITT photonic excitations with thermal excitations (dotted line). Repopulating the 3d- and 4s-bands in Cu causes a major difference in the values and temperature dependent trends in the electron-phonon coupling factor of Cu.

the integral in Eq. (11). In addition, the low-temperature values of $G(T_e)$ in the *ITT*-excited calculations are higher than the other calculations, which is due to the change in population of the s- band and d-bands due to interband transitions even at low temperatures. The calculations taking into account d-band thermal excitations follow the same trends as Lin et al. [20], but the values deviate as the d-band becomes thermally excited. This is ascribed to the differences between the exact band structure used by Lin et al. and the approximate band structure calculations used in this work. Therefore, using this band structure approximation, the computed trends in $G(T_e)$ are correct, but the values for each case should be considered an underestimate to the actual value of $G(T_e)$.

TRANSIENT CHANGE IN ELECTRON TEMPERATURE AND THE TWO-TEMPERATURE MODEL

In the event that the photonic excitation is in the form of a short laser pulse, the power of the laser pulse will be rapidly absorbed by the electrons in the metal creating a temperature difference between the electron and phonon systems (this, of course, assumes that the laser pulses are shorter than the electron-phonon equilibration time). In this case, the changes in the electron and phonon temperatures can be predicted with the two-temperature model, *TTM* [21]. When the metal film of interest is homogeneously heated (i.e., ballistic transport of electrons stretch out the thermal energy throughout the depth of the film creating minimal temperature gradient in the film after pulse absorption [5]), the *TTM* can be expressed as

$$C_e(T_e) \frac{\partial T_e}{\partial t} = -G(T_e)[T_e - T_L] + \frac{0.94A}{t_p d} \exp\left[-2.77\left(\frac{t - 2t_p}{t_p}\right)\right] \quad (17)$$

$$C_L \frac{\partial T_L}{\partial t} = G(T_e)[T_e - T_L] \quad (18)$$

where t is the time, A is the absorbed laser fluence, t_p is the pulse width, d is the film thickness, and the subscript L refers to the lattice, or phonon system. To properly consider the transient change in electron temperature after short pulse laser heating, the impact of photon energy $h\nu$ and subsequent transitions induced on the values $C_e(T_e)$ and $G(T_e)$ used in the evaluation of Eqs. (17) and (18) must be considered. In addition, the change in absorbed fluence will also depend on wavelength, but in these calculations, the value of A is used as an input. Figure 6 shows the transient change in electron temperature for a 20-nm Cu film at room temperature (300 K) after short pulse heating with a 150-fs pulse assuming a bulk value for the lattice specific heat, $C_L = 3.46 \times 10^6 \text{ J m}^{-3} \text{ K}^{-1}$ [29]. Three cases of absorbed fluence are considered, $A = 1$ (Figures 6a and 6b), 10 (Figures 6c and 6d), and 50 (Figures 6e and 6f) J m^{-2} . Figures 6a, 6c, and 6e show $T_e(t)$ as computed assuming d-band thermal excitations only when computing $C_e(T_e)$ and $G(T_e)$ compared to the predictions using the traditional assumptions used in the *TTM* of $C_e(T_e) = \gamma T_e$ and $G = G_0$. For direct comparison of the data sets, in calculations in Figure 6, G_0 is assumed as $G_0 = 5.56 \times 10^{16} \text{ W m}^{-3} \text{ K}^{-1}$, which is the low-temperature value from the numerical simulations in Figure 5, rather than G_0 from Eq. (6) discussed in the previous section. Figures 6b, 6d, and 6f

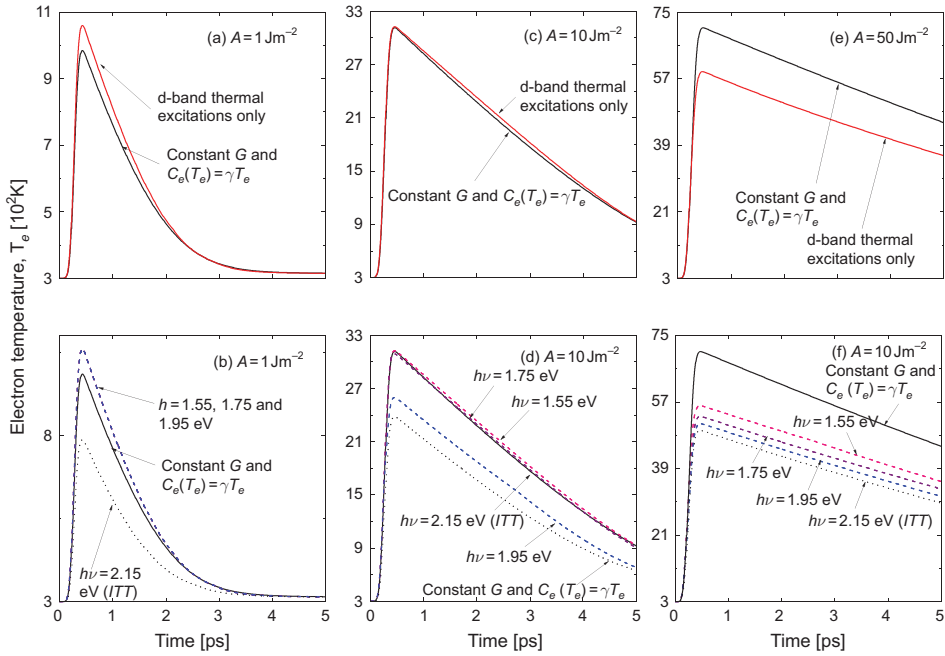


Figure 6. Transient changes in electron temperature for a 20-nm Cu film at room temperature (300 K) after short pulse heating with a 150-fs pulse. Three cases of absorbed fluence are considered, $A = 1$ (a) and (b); 10 (c) and (d); and 50 (e) and (f) J m^{-2} . (a), (c), and (e) show $T_e(t)$ as computed assuming d-band thermal excitations only when computing $C_e(T_e)$ and $G(T_e)$ compared to the predictions using the traditional assumptions used in the TTM of $C_e(T_e) = \gamma T_e$ and $G = G_0$. (b), (d), and (f) show $T_e(t)$ computed assuming the photonically induced interband transitions discussed in this work (with various values of $h\nu$) again compared to the predictions using the traditional assumptions used in the TTM of $C_e(T_e) = \gamma T_e$ and $G = G_0$.

show $T_e(t)$ computed assuming the photonically induced interband transitions discussed in this work (with various values of $h\nu$) again compared to the predictions using the traditional assumptions used in the TTM of $C_e(T_e) = \gamma T_e$ and $G = G_0$. Upon inducing interband transitions, the electron temperatures change, as expected from the changes in $C_e(T_e)$ and $G(T_e)$ from d- to s-band photonically excited interband transitions.

The changes in the maximum electron temperature are immensely important in determining electron-phonon scattering processes with ultrashort pulsed laser experiments. The wavelength of the incident laser pulse, which ultimately relates the reflected signal to the electron temperature, must be chosen appropriately in these experiments to determine the thermophysical properties. Large increases or changes in the measured signals could not only be from reflectivity changes around interband transitions but also from spikes in the electron temperature and changes in electron-phonon coupling rates due to electron relaxation. These processes must be considered when analyzing electron-phonon scattering with short pulsed lasers, especially at high absorbed fluences and large photonic energies.

CONCLUSIONS

This work examined the effects of thermally (Fermi smearing) and photonically (absorbed photon energy) induced d-band to Fermi level direct interband transitions on electron heat capacity and electron-phonon coupling factor calculations. The theory developed in the Theory section can be applied to all metals. The following section applies this theory to Cu to calculate the change in electron heat capacity and electron-phonon coupling factor as a function of temperature for various incident photon energies at and below the interband transition threshold. The final section presents calculations of the change in electron temperature as a function of time after short pulse absorption by a Cu film for various absorbed photon energies with the two temperature model. The results from this work give new insights into electron phonon scattering measurements with short pulsed lasers with photon energies that induce d-band to Fermi surface direct interband transitions.

This work focused on copper due to the relatively large d-band separation from the Fermi energy (typical of all noble metals). This same analysis can be applied to other metals, but the distinction of the onset of interband transitions will not be as clear in metals with a less distinct and smaller ITT , as mentioned in the Introduction. In fact, the d-bands in some metals overlap and have electron energies that are higher than the Fermi energy, as is apparent in the ab initio calculations of electron band structure by Lin et al. [20]. The overlapping of these d-bands with the Fermi energy yields an opposite effect on electron heat capacity and electron-phonon coupling factor from that observed in this work for noble metals. Therefore, it is expected that photonic excitations causing interband transitions in metals with d-band/Fermi energy overlap would also have an opposite effect on thermophysical properties from those trends observed in this work.

REFERENCES

1. A. Majumdar, K. Fushinobu, and K. Hijikata, Effect of Gate Voltage on Hot-Electron and Hot-Phonon Interaction and Transport in a Submicrometer Transistor, *Journal of Applied Physics*, vol. 77, pp. 6686–6694, 1995.
2. P.E. Hopkins and P.M. Norris, Substrate Influence in Electron-Phonon Coupling Measurements in Thin Au Films, *Applied Surface Science*, vol. 253, pp. 6289–6294, 2007.
3. A. Majumdar and P. Reddy, Role of Electron-Phonon Coupling in Thermal Conductance of Metal-Nonmetal Interfaces, *Applied Physics Letters*, vol. 84, pp. 4768–4770, 2004.
4. J. Hohlfeld, E. Matthias, R. Knorren, and K.H. Bennemann, Nonequilibrium Magnetization Dynamics of Nickel, *Physical Review Letters*, vol. 78, pp. 4861–4864, 1997.
5. J. Hohlfeld, S.-S. Wellershoff, J. Gudde, U. Conrad, V. Jahnke, and E. Matthias, Electron and Lattice Dynamics Following Optical Excitation of Metals, *Chemical Physics*, vol. 251, pp. 237–258, 2000.
6. D.S. Ivanov and L.V. Zhigilei, Combined Atomistic-Continuum Modeling of Short-Pulse Laser Melting and Disintegration of Metal Films, *Physical Review B*, vol. 68, Paper No. 064114, 2003.
7. Z. Lin and L.V. Zhigilei, Thermal Excitation of d Band Electrons in Au: Implications for Laser-Induced Phase Transformations, *High-Power Laser Ablation VI, Proc. SPIE*, vol. 6261, Paper No. 62610U, 2006.
8. Z. Lin and L.V. Zhigilei, Temperature Dependences of the Electron-Phonon Coupling, Electron Heat Capacity and Thermal Conductivity in Ni under Femtosecond Irradiation, *Applied Surface Science*, vol. 253, pp. 6295–6300, 2007.

9. S.-S. Wellershoff, J. Hohlfeld, J. Gudde, and E. Matthias, The Role of Electron-Phonon Coupling in Femtosecond Laser Damage of Metals, *Applied Physics A*, vol. 69, pp. S99–S107, 1999.
10. T.Q. Qiu and C.L. Tien, Size Effects on Nonequilibrium Laser Heating of Metal Films, *Journal of Heat Transfer*, vol. 115, pp. 842–847, 1993.
11. E. Colavita, A. Franciosi, C. Mariani, and R. Rosei, Thermoreflectance Test of W, Mo and Paramagnetic Cr Band Structures, *Physical Review B*, vol. 27, pp. 4684–4693, 1983.
12. J. Hanus, J. Feinleib, and W.J. Scouler, Low-Energy Interband Transitions and Band Structure in Nickel, *Physical Review Letters*, vol. 19, pp. 16–20, 1967.
13. P.E. Hopkins, J.M. Klopff, and P.M. Norris, Influence of Interband Transitions on Electron-Phonon Coupling Measurements in Ni Films, *Applied Optics*, vol. 46, pp. 2076–2083, 2007.
14. G.L. Eesley, Generation of Nonequilibrium Electron and Lattice Temperatures in Copper by Picosecond Laser Pulses, *Physical Review B*, vol. 33, pp. 2144–2151, 1986.
15. C. Kittel, *Introduction to Solid State Physics*, John Wiley & Sons, New York, 1996.
16. M.I. Kaganov, I.M. Lifshitz, and L.V. Tanatarov, Relaxation between Electrons and the Crystalline Lattice, *Soviet Physics JETP*, vol. 4, pp. 173–178, 1957.
17. G. Chen, *Nanoscale Energy Transport and Conversion: A Parallel Treatment of Electrons, Molecules, Phonons, and Photons*, Oxford University Press, New York, 2005.
18. C.S. Fadley and D.A. Shirley, X-Ray Photoelectron Spectroscopic Study of Iron, Cobalt, Nickel, Copper, and Platinum, *Physical Review Letters*, vol. 21, pp. 980–983, 1968.
19. A.N. Smith and P.M. Norris, Numerical Solution for the Diffusion of High Intensity, Ultrashort Laser Pulses within Metal Films, *Proceedings of the 11th International Heat Transfer Conference (Korean Society of Mechanical Engineers)*, vol. 5, p. 241, 1998.
20. Z. Lin, L.V. Zhigilei, and V. Celli, Electron-Phonon Coupling and Electron Heat Capacity of Metals under Conditions of Strong Electron-Phonon Nonequilibrium, *Physical Review B*, vol. 77, Paper No. 075133, 2008.
21. S.I. Anisimov, B.L. Kapeliovich, and T.L. Perel'man, Electron Emission from Metal Surfaces Exposed to Ultrashort Laser Pulses, *Soviet Physics - JETP*, vol. 39, pp. 375–377, 1974.
22. N.W. Ashcroft and N.D. Mermin, *Solid State Physics*, Saunders College, Fort Worth, TX, 1976.
23. Z. Zhang, *Nano/Microscale Heat Transfer*, McGraw-Hill, New York, 2007.
24. P.B. Allen, Theory of Thermal Relaxation of Electrons in Metals, *Physical Review Letters*, vol. 59, pp. 1460–1463, 1987.
25. S.D. Brorson, A. Kazeroonian, J.S. Moodera, D.W. Face, T.K. Cheng, E.P. Ippen, M.S. Dresselhaus, and G. Dresselhaus, Femtosecond Room-Temperature Measurement of the Electron-Phonon Coupling Constant λ in Metallic Superconductors, *Physical Review Letters*, vol. 64, pp. 2172–2175, 1990.
26. G. Grimvall, The Electron-Phonon Interactions in Metals, in E. Whohlfarth (ed.), *Selected Topics in Solid State Physics*, North-Holland, New York, 1981.
27. W.L. McMillan, Transition Temperature of Strong-Coupled Superconductors, *Physical Review*, vol. 167, pp. 331–344, 1968.
28. X.Y. Wang, D.M. Riffe, Y.-S. Lee, and M.C. Downer, Time-Resolved Electron-Temperature Measurement in a Highly Excited Gold Target Using Femtosecond Thermionic Emission, *Physical Review B*, vol. 50, pp. 8016–8019, 1994.
29. F. Incropera and D.P. DeWitt, *Fundamentals of Heat and Mass Transfer*, Wiley and Sons, New York, 1996.